# Supporting Information

# Varied spin crossover behaviour in a family of dinuclear Fe(II) triple helicate complexes

Rosanna J. Archer,[a,b] Hayley S. Scott,[a,b] Matthew I. J. Polson,[a] Bryce E. Williamson,[a] Corine Mathonière,[c,d] Mathieu Rouzières,[e,f] Rodolphe Clérac*[e,f] and Paul E. Kruger*[a,b]

a) School of Physical and Chemical Sciences, University of Canterbury, Private Bag 4800, Christchurch, 8140, New Zealand.

b) MacDiarmid Institute for Advanced Materials and Nanotechnology, School of Physical and Chemical Sciences, University of Canterbury, Private Bag 4800, Christchurch 8140, New Zealand. E-mail: paul.kruger@canterbury.ac.nz

c) CNRS, ICMCB, UMR 5026 F-33600 Pessac, France

d) Univ. Bordeaux, ICMCB, UMR 5026 F-33600 Pessac, France

e) CNRS, CRPP, UMR 5031 F-33600 Pessac, France
Email: clerac@crpp-bordeaux.cnrs.fr

f) Univ. Bordeaux, CRPP, UMR 5031 F-33600 Pessac, France

## Complexometric titration of L1 with $Fe(BF_4)_2{\cdot}6H_2O$ - Formation of a low-spin dinuclear triple helicate complex

In order to confirm the M:L stoichiometry and to probe the interaction between **L1** and Fe(II), a UV-vis. spectroscopic titration experiment was conducted (at 25°C) to follow the formation of **1**. An $CH_3CN$ solution of $Fe(BF_4)_2.6H_2O$ ($1.084\times10^{-3}$ M) was added in 10 µL aliquots to a 3 mL $CH_3CN$ solution of **L1** ($6.410\times10^{-5}$ M). After each addition the UV-vis. spectrum was recorded. The absorbance spectrum of **L1** revealed one major peak in the UV region with a maximum absorbance ($\lambda_{max}$) occurring at 261 nm ($\varepsilon$ = 35700 ± 100 L mol$^{-1}$ cm$^{-1}$). This is consistent with the highly conjugated nature of the ligand system and can be attributed to a π-π* transition. As aliquots of Fe(II) were added, a broad absorption band formed between 500-600 nm, with $\lambda_{max}$ = 570 nm ($\varepsilon$ = 10700 ± 100 L mol$^{-1}$ cm$^{-1}$) and this is assigned to the MLCT. Tight isosbestic points are observed at 243 and 357 nm indicating a transition from the uncoordinated ligand to an $[Fe_2\mathbf{L1}_3]^{4+}$ complex. Upon coordination to the metal centre the π-π* transition at 261 nm undergoes a red-shift of nearly 30 nm to reach a $\lambda_{max}$ value of 287 nm at the end of the titration, as displayed in **Figure S1**.

By plotting the absorbance at 570 nm against the molar ratio ([Fe(II)]/[**L1**]), it is clear that the stoichiometry for the formation of **1** is 3**L1**:2Fe as anticipated (**Figure S1** inset). Addition of further $Fe(BF_4)_2{\cdot}6H_2O$ did not alter the absorbance once this stoichiometry was reached. The intense deep purple colour and the formation of a substantial MLCT transition band during the UV-vis. titration of **1** is consistent with a [LS-LS] electronic configuration for the complex at this temperature.

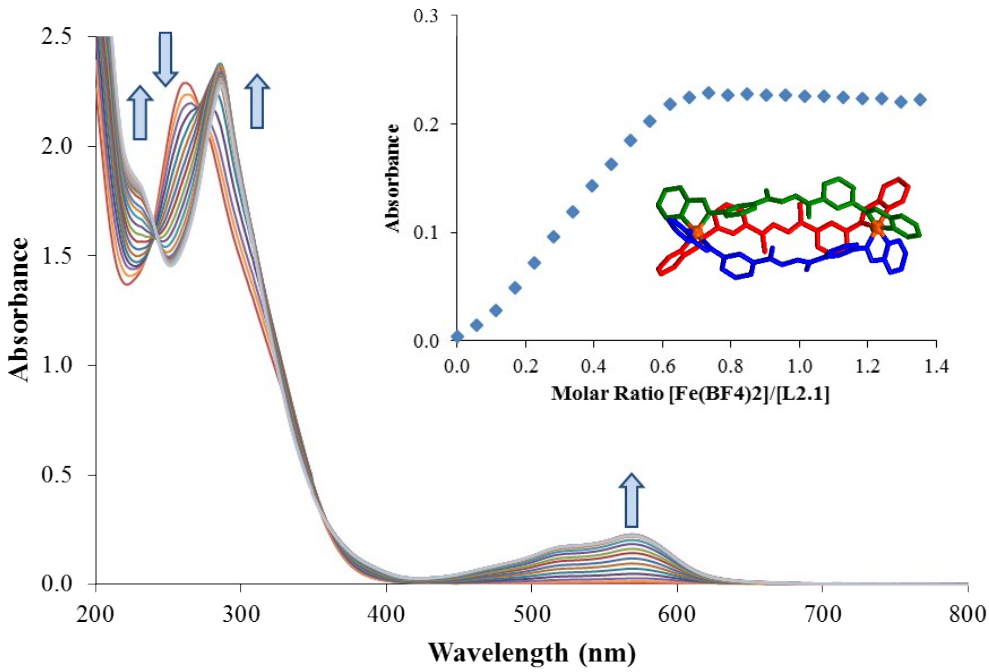


**Figure S1.** UV-Visible spectroscopic complexometric titration of $Fe(BF_4)_2{\cdot}6H_2O$ ($1.084\times10^{-3}$ mol L$^{-1}$) against **L1** ($6.410\times10^{-5}$ mol L$^{-1}$) in $CH_3CN$. Inset: Absorbance vs. molar ratio at 570 nm and structure showing the $[Fe_2\mathbf{L1}_3]^{4+}$ dinuclear helicate.

**X-ray crystallographic data refinement on 1-3**

For compound **1**, following the identification of four $BF_4^-$ anions, $H_2O$, $CH_3CN$ and $CHCl_3$ solvent molecules a solvent mask was applied as the remaining electron density within **1** could not be used to accurately model further solvent molecules. Structural data obtained for **3** were of low quality owing to the inherent weakly diffracting nature of crystals. Multiple crystals of **3** were measured in attempts to improve quality of the data, however, in all cases the data were poor. For compound **3** collected at 120 K, one of the $BF_4^-$ anions has been modelled as isotropic and disordered over two position (both of which have been assigned half occupancy). DFIX and DANG restraints have been placed on the disordered anion. Following the identification of one $CH_3CN$, one $CHCl_3$ and one half of a $H_2O$ molecule, the solvent mask was applied as no further solvent could be identified. For compound **3** collected at 240 K, three $BF_4^-$ anions have been refined isotropically as the fluorine atoms on the anions had large $U_{eq}$ due to increased thermal motion which could not be easily modelled. A solvent mask was applied to the structure following identification of a $CHCl_3$ and a $H_2O$ solvent molecule. Owing to the poor structural quality of compound **3** (at 120 and 240 K) hydrogen bonding parameters which include solvents and anions have not been reported.

## Crystallographic Details

**Table S1.** Crystallographic data for **1** and **2** at 120 K.

| Compound reference | **1** | **2** |
|---|---|---|
| Chemical formula | $[C_{84}H_{72}Fe_2N_{18}](BF_4)_4$•$CHCl_3$•$H_2O$•$2(C_2H_3N)$ | $[C_{72}H_{66}Fe_2N_{24}](BF_4)_4$•$1.5CH_3CN$ |
| Formula Mass | 2010.0 | 1789.52 |
| Crystal system | Monoclinic | Orthorhombic |
| *a* /Å | 27.8736(8) | 18.3905(4) |
| *b* /Å | 28.1738(6) | 22.6878(9) |
| *c* /Å | 14.1358(3) | 19.0917(6) |
| $\alpha$ /° | 90.00 | 90.00 |
| $\beta$ /° | 114.960(2) | 90.00 |
| $\gamma$ /° | 90.00 | 90.00 |
| Unit cell volume /Å$^3$ | 10064.1(4) | 7965.8(4) |
| Temperature /K | 120.0(2) | 119.99(10) |
| Space group | *C2/c* | *Pccn* |
| No. of formula units per unit cell, *Z* | 4 | 4 |
| No. of reflections measured | 19623 | 33396 |
| No. of independent reflections | 9886 | 7964 |
| $R_{int}$ | 0.0352 | 0.0386 |
| Final $R_1$ values ($I > 2\sigma(I)$) | 0.0807 | 0.0879 |
| Final $wR(F^2)$ values ($I > 2\sigma(I)$) | 0.2329 | 0.22606 |
| Final $R_1$ values (all data) | 0.0964 | 0.1277 |
| Final $wR(F^2)$ values (all data) | 0.2505 | 0.3020 |

## Variable temperature X-ray crystallographic data collection on 3

The crystal data for **3** was first collected at 120 K and following refinement and subsequent inspection of the Fe-N bond lengths, it was noted that the data were consistent with a predominantly [LS-HS] electronic configuration about the Fe-centres. To ascertain whether the [HS-HS] state could be obtained, the same crystal was heated slowly on the diffractometer within the $N_2$ cold-stream (1K/min) to 240K (higher temperatures led to significant crystal deterioration, presumably due to solvent loss). Once the crystal had equilibrated at 240K, a second full data collection was obtained. The data obtained at each temperature was solved and refined in the same triclinic $P\bar{1}$ space group. From the data solution for that obtained at 240K it was noted some partial desolvation of the crystal had also occurred, see Table S2.

**Table S2.** Crystallographic Data for **3** at 120 and 240 K.

| Compound reference | **3 -120 K** | **3' - 240 K** |
|---|---|---|
| Chemical formula | $[C_{72}H_{66}Fe_2N_{24}](BF_4)_4$•$CHCl_3$•$CH_3CN$•$0.5H_2O$ | $[C_{72}H_{66}Fe_2N_{24}](BF_4)_4$•$0.5CHCl_3$•$H_2O$ |
| Formula Mass | 1894.85 | 1819.83 |
| Crystal system | Triclinic | Triclinic |
| $a$ /Å | 13.9106(5) | 14.1516(9) |
| $b$ /Å | 15.9337(6) | 16.1395(8) |
| $c$ /Å | 24.8612(9) | 24.9544(11) |
| $\alpha$ /° | 73.547(3) | 73.358(4) |
| $\beta$ /° | 75.732(3) | 76.332(5) |
| $\gamma$ /° | 73.498(3) | 73.466(5) |
| Unit cell volume /Å$^3$ | 4983.8(3) | 5160.2(5) |
| Temperature /K | 120.0(1) | 240.43(10) |
| Space group | $P\bar{1}$ | $P\bar{1}$ |
| No. of formula units per unit cell, $Z$ | 2 | 2 |
| No. of reflections measured | 34551 | 37020 |
| No. of independent reflections | 17779 | 20325 |
| $R_{int}$ | 0.0604 | 0.0738 |
| Final $R_1$ values ($I > 2\sigma(I)$) | 0.0832 | 0.1484 |
| Final $wR(F^2)$ values ($I > 2\sigma(I)$) | 0.2333 | 0.3795 |
| Final $R_1$ values (all data) | 0.1043 | 0.1987 |
| Final $wR(F^2)$ values (all data) | 0.2546 | 0.4516 |

**Table S3.** Selected coordination bond lengths and angles for **1-3**.

| **Bond Lengths (Å)** | | **Bond Angles (°)** | | | |
|---|---|---|---|---|---|
| Compound **1** (120 K) | | | | | |
| **Fe1-N1** | 1.983(3) | **N1-Fe1-N2** | 80.92(13) | **N2-Fe1-N8** | 96.96(13) |
| **Fe1-N2** | 1.979(3) | **N1-Fe1-N6** | 91.22(13) | **N5-Fe1-N6** | 81.20(13) |
| **Fe1-N5** | 1.971(3) | **N1-Fe1-N7** | 94.34(14) | **N5-Fe1-N7** | 91.26(13) |
| **Fe1-N6** | 1.989(3) | **N1-Fe1-N8** | 91.61(13) | **N5-Fe1-N8** | 96.37(13) |
| **Fe1-N7** | 1.971(3) | **N2-Fe1-N5** | 93.71(13) | **N6-Fe1-N7** | 94.12(13) |
| **Fe1-N8** | 1.993(3) | **N2-Fe1-N6** | 88.11(13) | **N7-Fe1-N8** | 81.00(13) |
| | | | | | |
| Compound **2** (120 K) | | | | | |
| **Fe1-N1** | 1.948(5) | **N1-Fe1-N3** | 80.4(2) | **N3-Fe1-N11** | 98.92(18) |
| **Fe1-N3** | 2.005(4) | **N1-Fe1-N8** | 93.0(2) | **N6-Fe1-N8** | 80.67(19) |
| **Fe1-N6** | 2.003(5) | **N1-Fe1-N9** | 92.8(2) | **N6-Fe1-N9** | 92.51(19) |
| **Fe1-N8** | 1.958(5) | **N1-Fe1-N11** | 88.7(2) | **N6-Fe1-N11** | 98.2(2) |
| **Fe1-N9** | 1.960(5) | **N3-Fe1-N6** | 94.34(19) | **N8-Fe1-N9** | 92.62(19) |
| **Fe1-N11** | 2.015(5) | **N3-Fe1-N8** | 88.12(19) | **N9-Fe1-N11** | 80.45(19) |
| | | | | | |
| Compound **3** (120 K) | | | | | |
| **Fe1-N1** | 1.984(4) | **N1-Fe1-N3** | 80.37(15) | **N6-Fe2-N7** | 78.46(16) |
| **Fe1-N3** | 2.044(4) | **N1-Fe1-N9** | 93.61(16) | **N6-Fe2-N14** | 97.79(15) |
| **Fe1-N9** | 1.960(4) | **N1-Fe1-N17** | 92.32(16) | **N6-Fe2-N22** | 92.34(14) |
| **Fe1-N11** | 2.036(4) | **N1-Fe1-N19** | 86.58(15) | **N6-Fe2-N23** | 86.10(16) |
| **Fe1-N17** | 1.988(4) | **N3-Fe1-N9** | 93.49(15) | **N7-Fe2-N14** | 96.03(16) |
| **Fe1-N19** | 2.022(4) | **N3-Fe1-N11** | 96.73(14) | **N7-Fe2-N16** | 95.89(17) |
| **Fe2-N6** | 2.119(4) | **N3-Fe1-N19** | 93.81(14) | **N7-Fe2-N23** | 90.14(17) |
| **Fe2-N7** | 2.048(4) | **N9-Fe1-N11** | 80.48(15) | **N14-Fe2-N16** | 78.67(17) |
| **Fe2-N14** | 2.114(4) | **N9-Fe1-N17** | 93.00(16) | **N14-Fe2-N22** | 96.01(14) |
| **Fe2-N16** | 2.046(6) | **N11-Fe1-N17** | 93.00(16) | **N16-Fe2-N22** | 93.96(16) |
| **Fe2-N22** | 2.119(4) | **N11-Fe1-N19** | 99.69(15) | **N16-Fe2-N23** | 98.02(18) |
| **Fe2-N23** | 2.066(4) | **N17-Fe1-N19** | 79.62(15) | **N22-Fe2-N23** | 78.26(15) |

| Bond Lengths (Å) | | Bond Angles (°) | | | |
|---|---|---|---|---|---|
| Compound **3'** (240 K) | | | | | |
| **Fe1-N1** | 2.156(7) | **N1-Fe1-N3** | 77.0(2) | **N6-Fe2-N7** | 76.6(3) |
| **Fe1-N3** | 2.234(6) | **N1-Fe1-N9** | 101.4(3) | **N6-Fe2-N14** | 100.8(2) |
| **Fe1-N9** | 2.165(6) | **N1-Fe1-N11** | 94.7(2) | **N6-Fe2-N15** | 93.3(3) |
| **Fe1-N11** | 2.257(7) | **N1-Fe1-N17** | 98.4(3) | **N6-Fe2-N22** | 94.3(2) |
| **Fe1-N17** | 2.129(7) | **N3-Fe1-N11** | 95.4(2) | **N7-Fe2-N15** | 96.6(3) |
| **Fe1-N19** | 2.238(6) | **N3-Fe1-N17** | 98.3(2) | **N7-Fe2-N22** | 96.3(3) |
| **Fe2-N6** | 2.214(6) | **N3-Fe1-N19** | 97.0(2) | **N7-Fe2-N23** | 97.3(3) |
| **Fe2-N7** | 2.169(6) | **N9-Fe1-N11** | 91.0(2) | **N14-Fe2-N15** | 75.9(3) |
| **Fe2-N14** | 2.218(6) | **N9-Fe1-N17** | 89.8(3) | **N14-Fe2-N22** | 91.4(2) |
| **Fe2-N15** | 2.138(8) | **N9-Fe1-N19** | 85.3(2) | **N14-Fe2-N23** | 86.4(2) |
| **Fe2-N22** | 2.255(6) | **N11-Fe1-N19** | 91.0(2) | **N15-Fe2-N23** | 96.3(3) |
| **Fe2-N23** | 2.131(6) | **N17-Fe1-N19** | 77.2(3) | **N22-Fe2-N23** | 77.3(2) |

**Table S4.** Hydrogen bonding parameters for **2**.

| D-H···A | d (D-H) Å | d (D-H···A) Å | d (D···A) Å | < (D-H···A) ° | Symmetry Code |
|---|---|---|---|---|---|
| N2-H2···F7[1] | 0.89(2) | 2.088(4) | 2.797(7) | 139(5) | (1) x+1/2, -y-1, -z-1/2 |
| N2-H2···N13[2] | 0.89(2) | 2.45(5) | 2.966(11) | 119(4) | (2) x, -y-1/2, z +1/2 |
| N7-H7···F3 | 0.89(2) | 1.96(5) | 2.761(7) | 153(7) | (3) –x-1, -y-1, -z-1 |
| N10-H10···F6 | 0.86(2) | 2.12(4) | 2.779(8) | 132(6) | (4) –x-3/2, y, z+1/2 |

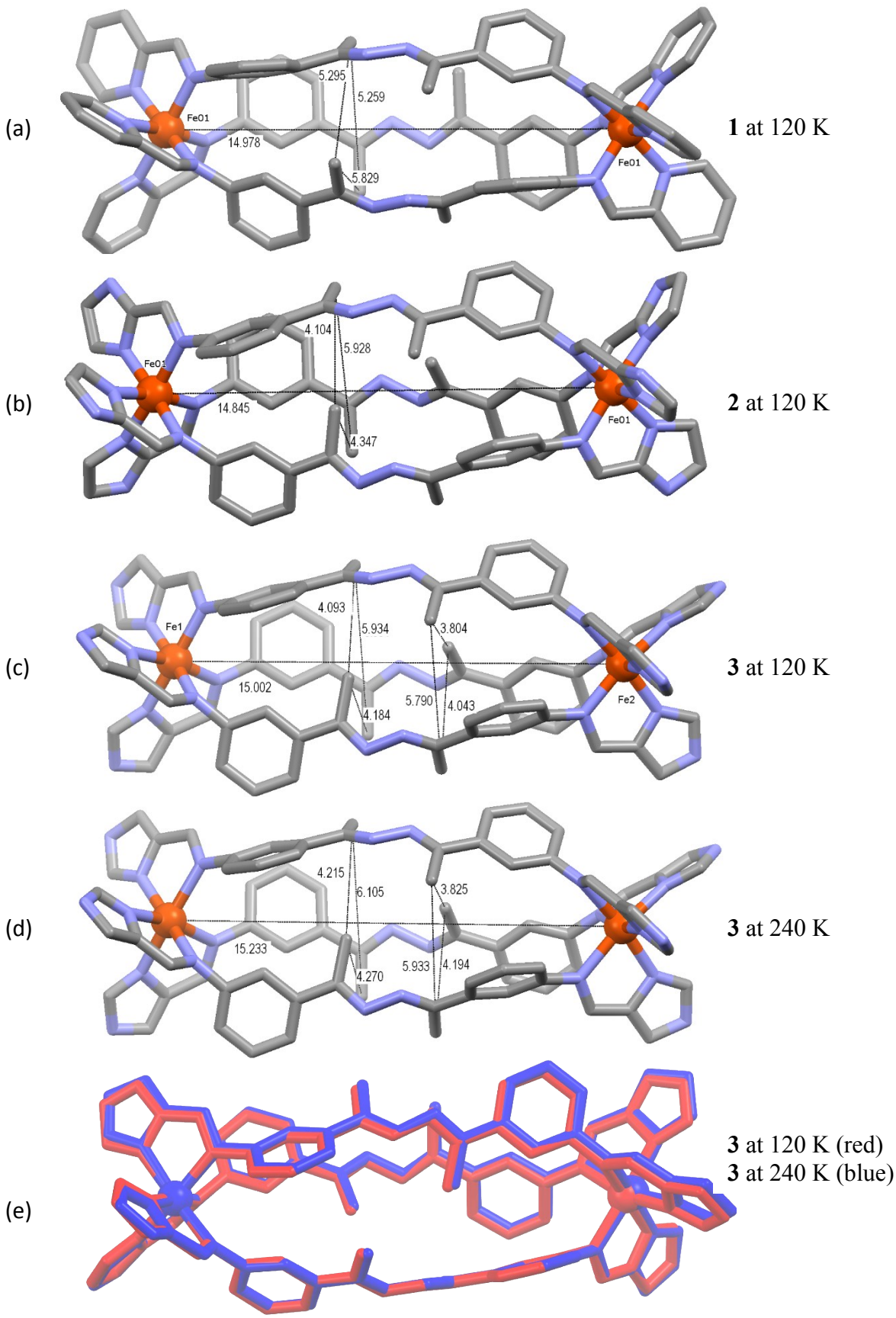


**Figure S2.** (a)-(d) Selected geometric parameters (Å) for **1-3** and (e) overlay of **3** at 120 (red) and 240 K (blue). Hydrogen atoms, solvent molecules and anions omitted for clarity.

**Crystal packing in 1-3**

Despite the similarities in helicate structure between the three complexes, all three structures show different crystal packing behaviour.

In **1**, packing between adjacent helicate units is propagated via face-to-face and edge-to-face π-type interactions as shown in Figure S3. There are no significant interactions involving the anions.

In **2**, the imidazole N-H groups act as hydrogen bond donors towards the $BF_4^-$ counter-anions. Two symmetry equivalent $BF_4^-$ counter-anions bridge two complexes through hydrogen bonding interactions between N2-H2···F7 and N10-H10···F6, as shown in Figure S4. The other $BF_4^-$ counter-anions hydrogen bond to the remaining hydrogen bond donor through N7-H7···F3 but no further hydrogen bonding occurs to this $BF_4^-$. A table outlining the hydrogen bonding parameters is provided in Table S4. The hydrogen bonding interactions extend to form a supramolecular chain of helices parallel to the [1,1,0] crystallographic plane. Both helical enantiomers are present within the crystal lattice and the helices are alternately inverted along the hydrogen bonding chain. The 2-fold screw axis causes two of the hydrogen bonding chains to lie perpendicular to one another, so that a helicate effectively sits in the groove within the hydrogen bonding network. In this packing arrangement, solvent accessible channels exist which run parallel to the crystallographic *c*-axis. The equivalent of 1.5 acetonitrile molecules per helicate reside in this channel, with one lying directly on a 2-fold rotation symmetry axis. The channels are approximately 6 Å × 6 Å in diameter. The crystals of **2** appeared to maintain single crystallinity through gentle drying processes, however, structural analysis of the dried compound *via* X-ray diffraction was unsuccessful with only weak diffraction of the sample being observed. Likewise, attempts to obtain higher temperature (*ca.* 240 K) data collection also met with failure due to very weak diffraction and loss of crystallinity.

In **3**, the packing showed similar interhelical interactions to those observed in **1**. Inspection of the crystal lattice reveals interhelical edge-to-face C-H···π interactions that extend from each of the three ligand strands of the complex with C-H···π(centroid) distances of 2.699(2) Å and 2.717(2) Å respectively. These interactions form a 2D sheet, which extends parallel to the crystallographic *a*- and *b*-axes, as shown in Figure S5. The $BF_4^-$ counter-anions are located towards the ends of the helicates and form hydrogen bonding interactions with the imidazole N-H moieties with D···A distances ranging between 2.75(2) Å and 3.00(1) Å. These interactions join the 2D-networks in the third dimension along the crystallographic *c*-axis, Figure S5. The packing results in pockets within the crystal lattice that contain disordered solvent molecules which were modelled as three chloroform molecules disordered over four positions, 1.5 molecules of acetonitrile, and the equivalent of one water molecule in two partially occupied positions. The crystal packing at 240 K showed no major alterations to the interactions between helicates within the crystal lattice, Figure S6. Interhelical Fe-Fe distances between helicates within the 2D-sheet lie within the range 9.386(2) – 9.629(2) Å at 240 K compared with 9.331(1) – 9.398(1) Å at 120 K. The longer distances coincide with the expansion of the unit cell along the crystallographic *a*- and *b*- axes.

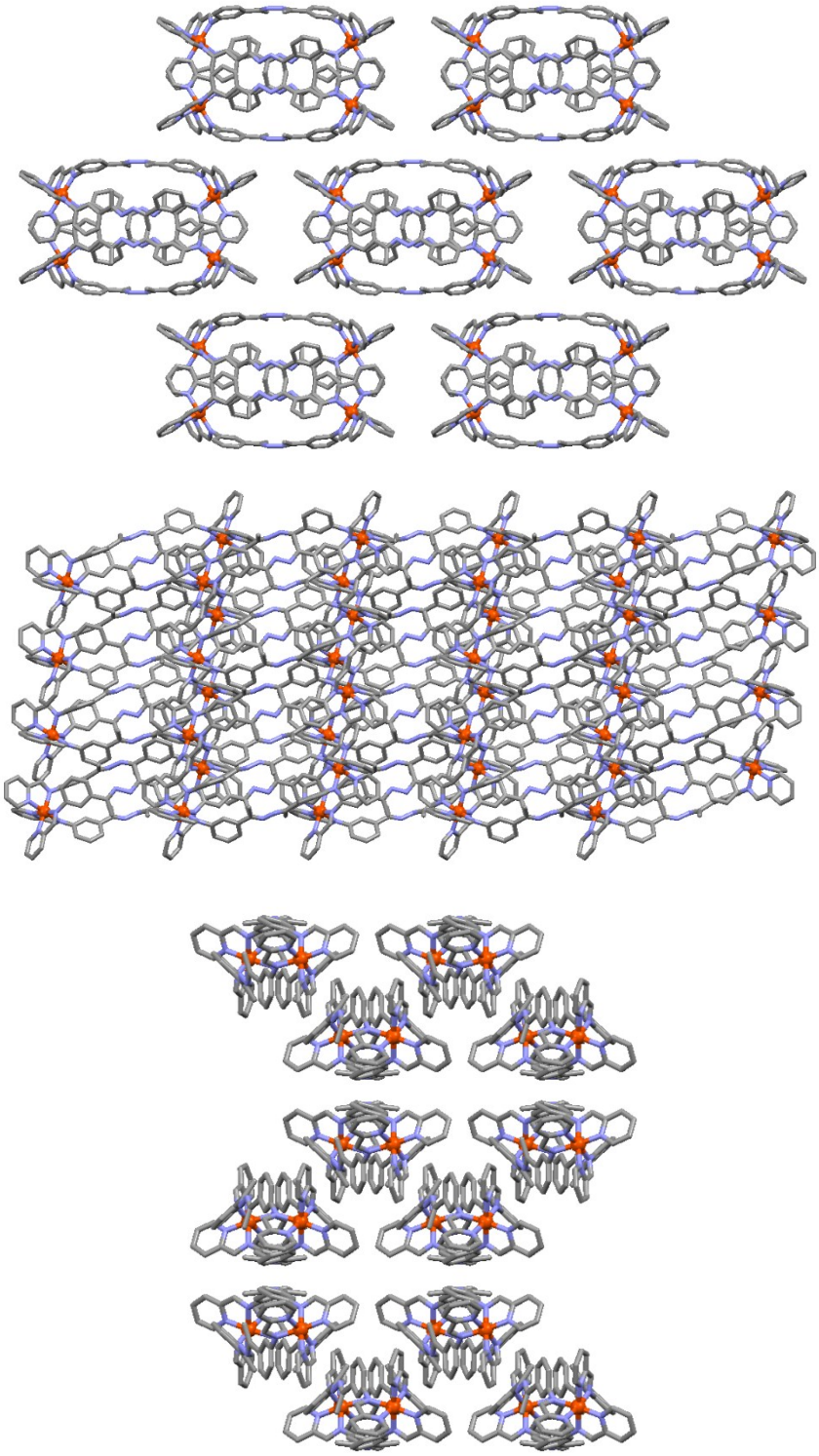

**Figure S3.** Crystal packing in **1** looking down the crystallographic *a*- (top), *b*- (middle) and *c*-axes (bottom) at 120 K. Counter-anions, solvent molecules and hydrogen atoms have been omitted for clarity.

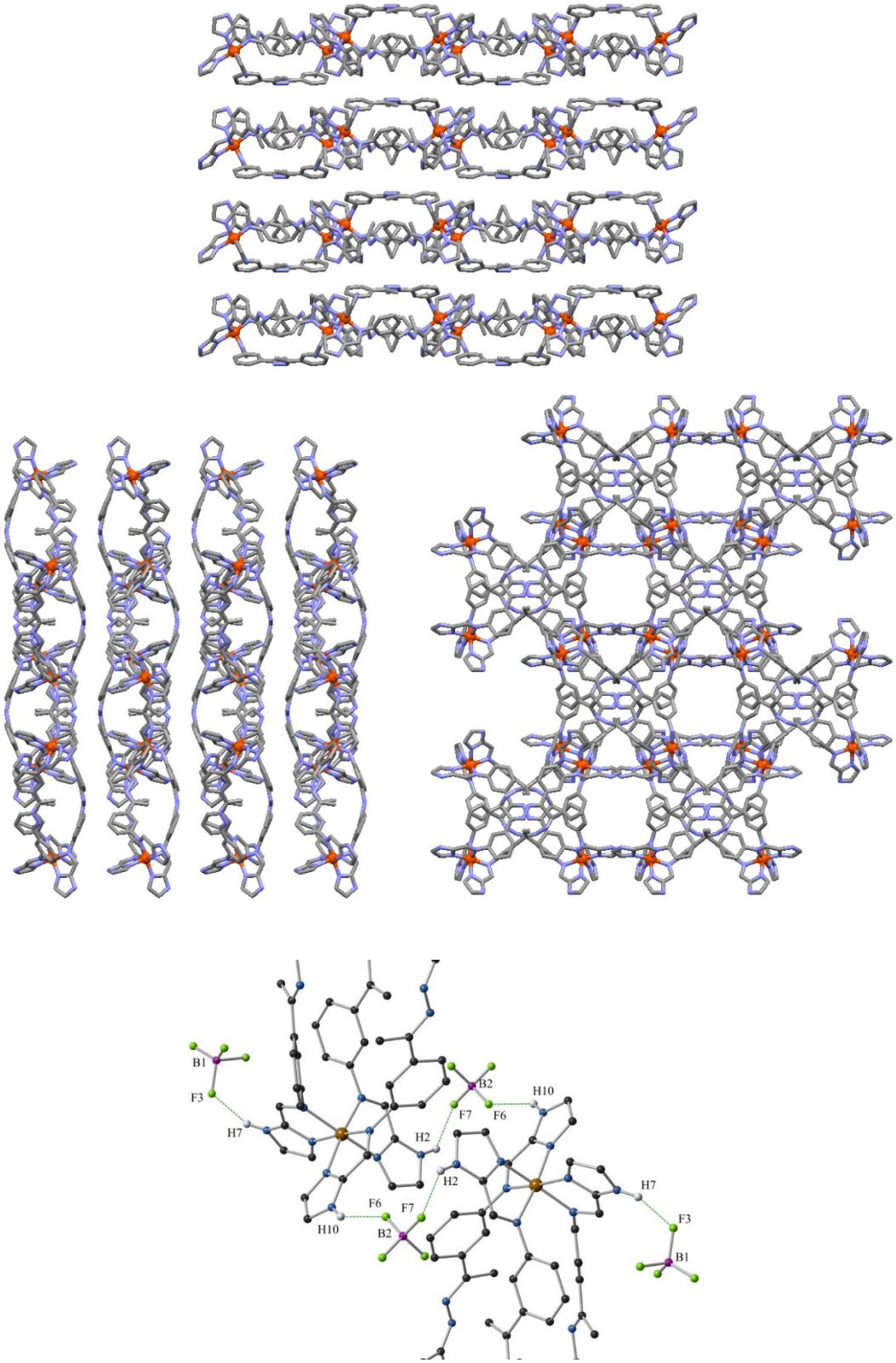


**Figure S4.** Crystal packing in **2** looking down the crystallographic *a*- (top), *b*- (middle, left) and *c*- axes (middle, right) at 120 K. Counter-anions, solvent molecules and hydrogen atoms have been omitted for clarity. Detail showing hydrogen bonding interactions involving the imidazole N-H and $BF_4^-$ counter-anions (bottom).

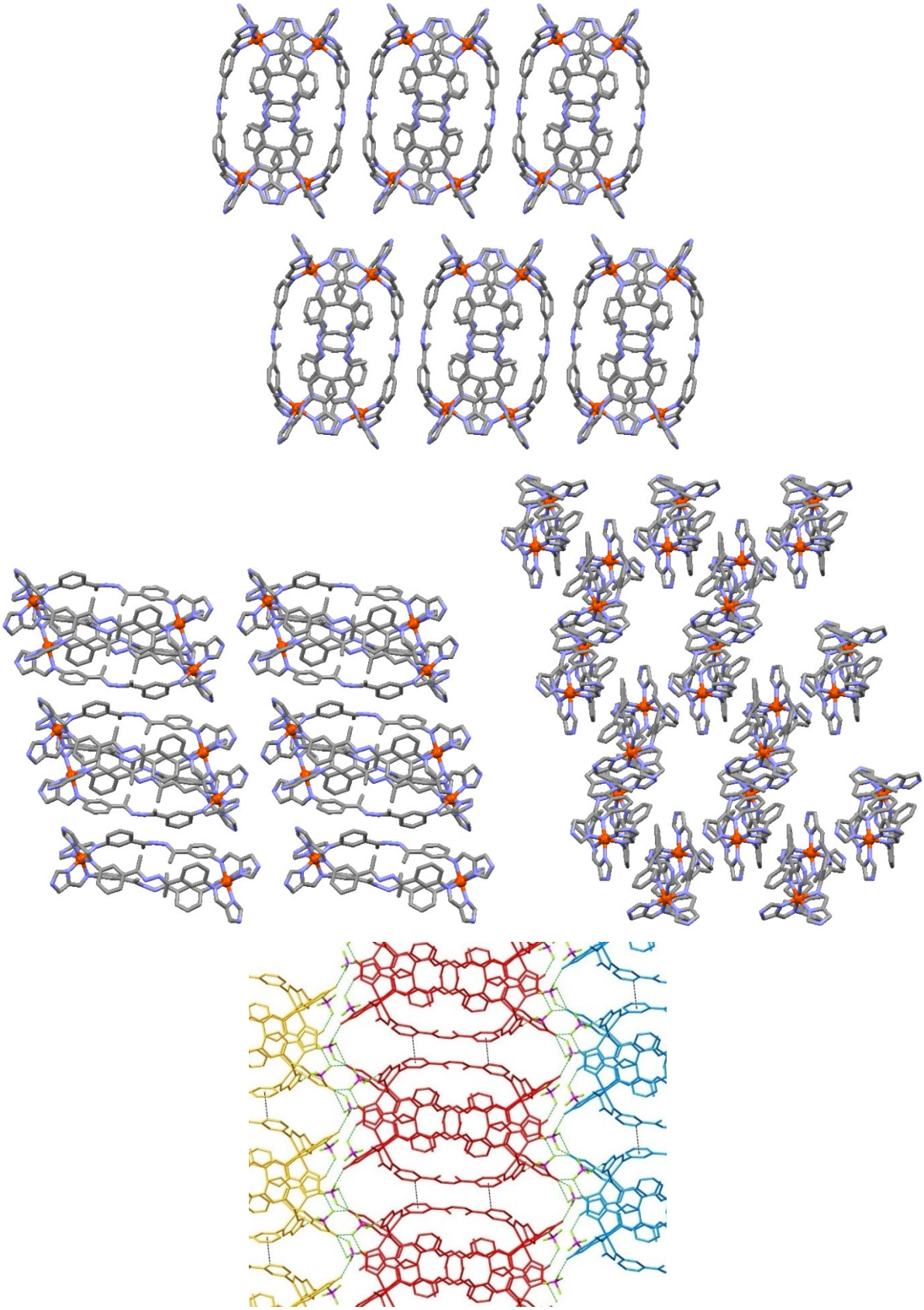

**Figure S5.** Crystal packing in **3** looking down the crystallographic *a*- (top), *b*- (middle, left) and *c*- axes (middle, right) at 120 K. Counter-anions, solvent molecules and hydrogen atoms have been omitted for clarity. Detail showing hydrogen bonding interactions involving the imidazole N-H and $BF_4^-$ counter-anions (bottom).

## Variable temperature UV-vis measurements on complex 2

$$\frac{A}{cl} = \varepsilon_{LS} + \frac{\varepsilon_{HS} - \varepsilon_{LS}}{1 + exp\left(\frac{\Delta H^{\circ}}{R}\left(\frac{1}{T} - \frac{1}{T_{1/2}}\right)\right)} \qquad Eqn.\ S1$$

Model derived to fit the data assuming the van't Hoff equation and the Beer-Lambert law. Definitions of parameters: $A$ = absorbance; $c$ = total concentration of solution; $l$ = path length (1 cm); $\varepsilon_{LS}$ and $\varepsilon_{HS}$ = molar absorption coefficients for the low-spin (LS) and high-spin (HS) states respectively; $\Delta H°$ = enthalpy associated with the SCO process in solution; $T$ = temperature; $T_{1/2}$ = temperature at which concentrations of HS and LS states are equal; $R$ = gas constant 8.314 J mol$^{-1}$ K$^{-1}$.

## Surface reflectivity measurements

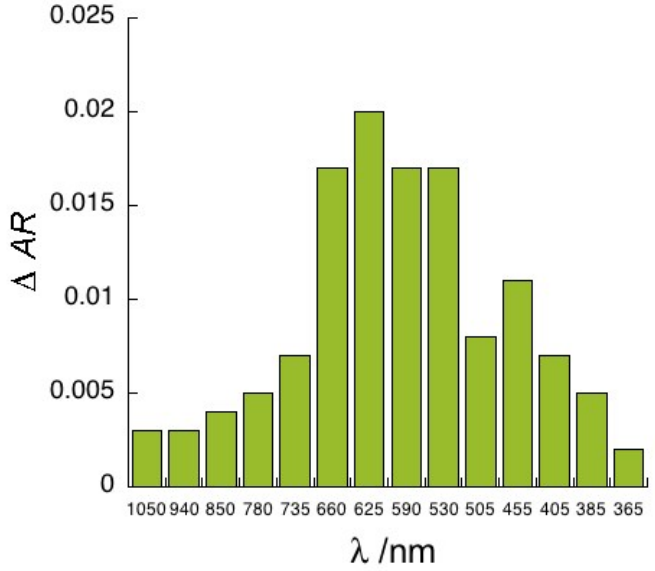


**Figure S6.** Relative change, Δ*AR*, in the absolute reflectivity at 900 nm ($R_{900}$) for **2** under different LED light conditions. Green light of 530 nm was selected for subsequent experiments.

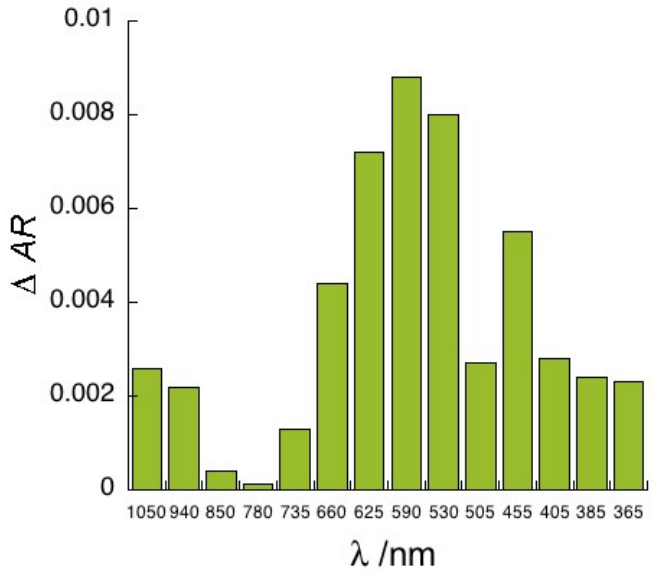


**Figure S7.** Relative change, Δ*AR*, in the absolute reflectivity at 900 nm ($R_{900}$) for **3** under different LED light conditions. Green light of 530 nm was selected for subsequent experiments.

## References


S1. G. M. Sheldrick, *Acta Crystallogr., Sect. A*, 2008, **64**, 112-122

S2. G. M. Sheldrick, SHELXL-97, Programs for X-ray Crystal Structure Refinement, 1997, University of Gottingen.

S3. O. V. Dolomanov, L. J. Bourhis, R. J. Gildea, J. A. K. Howard, H. J. Puschmann, *Appl. Cryst*. 2009, **42**, 339-341.